JPE 18-5-12

https://doi.org/10.6113/JPE.2018.18.5.1424
ISSN(Print): 1598-2092 / ISSN(Online): 2093-4718

Decoupled SVPWM for Five-Phase Permanent Magnet Machines with Trapezoidal Back-EMF

Zhipeng Lin*, Guohai Liu*, Wenxiang Zhao*, and Qian Chen†

†,*School of Electrical and Information Engineering, Jiangsu University, Jiangsu, China

Abstract

This paper presents a novel space vector pulse-width modulation (SVPWM) to synthesize an arbitrary non-sinusoidal phase voltage. The key of the proposed method is that the switching vectors used to comprise the reference vectors in the α_1-β_1 frame and the α_3-β_3 frame are decoupled. In the α_1-β_1 frame, the reference vector is comprised by near two large vectors. The corresponding vector comprised by the two vectors in the α_3-β_3 frame is considered as a disturbance, which is restrained by close-loop control. In the α_3-β_3 frame, there are two methods to comprise the reference vector. Method I is a near two middle vectors method. Method II uses near four vectors (two middle and two little vectors). The proposed SVPWM using decoupled switching vectors can guarantee a maximum modulation index in the α_1-β_1 frame. The effectiveness of the proposed method is verified by simulated and experimental results under various operation conditions.

Key words: Decoupled concept, Five-phase permanent magnet machine, Non-sinusoidal voltage, Space vector pulse-width modulation (SVPWM), Trapezoidal back-EMF

I. INTRODUCTION

Multi-phase machines have been widely used in a variety of industrial applications for the last decade, due to their intrinsic features such as power splitting, better fault tolerance and lower torque ripple than three-phase machines [1]-[5]. During the design process, some five-phase permanent magnet (PM) machines are designed to have non-sinusoidal back-EMF in order to increase the maximum output torque [6]-[9]. In [6] and [7], harmonics are injected into the PM shape to maximize the output torque in five-phase PM machines. To realize the maximize output torque of five-phase machines with trapezoidal back-EMF, third harmonic current injection methods have been proposed in [10]-[14]. In order to improve the torque of five-phase unequal tooth surface-mounted PM machines, third harmonic currents are injected into the stator windings based on the ratio of the third harmonic back-EMF to the fundamental one [10]. A bifurcation analysis of a five-phase induction machine when a third harmonic is injected for torque-enhancement has been proposed in [11]. In [12], experimental results show that the output torque after an injection of the third harmonic current in a five-phase induction machine with trapezoidal back-EMF can increase by 11% when compared with only using the fundamental current.

In five-phase space vector pulse-width modulation (SVPWM) methods, the traditional near two large vectors method produces the harmonic vector and current in α_3-β_3 frame, due to the vector in α_3-β_3 frame without control [15]. In order to realize a sinusoidal phase voltage, near four vectors methods have been proposed in [16]-[18]. In [18], two SVPWM methods are proposed to reduce common-mode voltage. In [19], the method proposed in [18] was extended to the over-modulation zone. M. Jones [20] investigated the stator current ripple, caused by the switching harmonics, under two SVPWM techniques in which two large and two medium vectors or four large vectors are used. However, these methods only focus on how to produce a sinusoidal voltage. Based on a multiple *d-q* space concept, a novel analysis of a multiphase SVPWM for synthesizing an arbitrary non-sinusoidal phase voltage has been proposed in [21]. This method can comprise the reference voltages by near four vectors in the α_1-β_1 frame and the α_3-β_3 frame. However, the near four vectors used to comprise the reference vectors in the α_1-β_1 frame and the α_3-β_3 frame are coupled.

Manuscript received Mar. 17, 2018; accepted Jul. 15, 2018
Recommended for publication by Associate Editor Zheng Wang.
†Corresponding Author: chenqian0501@ujs.edu.cn
Tel: +86-15252900600, Fax: +86-051188787773, Jiangsu University
*School of Electrical and Information Engineering, Jiangsu University, China

In this paper, a novel SVPWM is presented to synthesize a non-sinusoidal phase voltage. In the α_1-β_1 frame, the reference vector is comprised by near two large vectors to guarantee the maximum voltage linear output area. The corresponding vector comprised by two vectors in the α_3-β_3 frame is considered as a disturbance, which is restrained by a close-loop control. In the α_3-β_3 frame, there are two methods for comprising the reference voltage. For Method I, near two middle vectors are used to maintain the maximum voltage linear output area in the α_3-β_3 frame. For Method II, near four vectors (two middle and two little vectors) are adopted to improve the robustness of the system on the basis of ensuring the maximum modulation index in the α_1-β_1 frame. In the proposed method, the switching vectors used to comprise the reference vectors in the α_1-β_1 frame and the α_3-β_3 frame are decoupled, which can guarantee the maximum modulation index in the α_1-β_1 frame.

II. Motor Topology and Mathematical Model

Fig. 1 shows a 20-slot/18-pole five-phase PM machine [22]. It adopts an outer-rotor topology to achieve the prominent dynamic performance of electric vehicles, which can enhance its torque capability. Fig. 2 shows the measured back-EMF of a machine and fast Fourier transform results of measured back-EMF data. It is found that the back-EMF of a machine contains 22.2% third harmonic, 9.6% fifth harmonic and 1.2% seventh harmonic. The amplitude and phase of the fifth harmonic flux linkages are the same. Since the sum of the five-phase current is zero under a star connection, the fifth harmonic flux linkages do not produce torque and can be ignored. To simplify the mathematical model of a five-phase PM machine, only the fundamental and third harmonic components are considered. The parameters of a five-phase PM machine are listed in Table I.

The back-EMFs are produced by the magnetic flux linkages, and the magnetic flux linkages of a five-phase PM machine are presented as follows:

$$\psi_m = \psi_{m1}\begin{bmatrix}\cos\theta_e\\ \cos(\theta_e-\delta)\\ \cos(\theta_e-2\delta)\\ \cos(\theta_e-3\delta)\\ \cos(\theta_e-4\delta)\end{bmatrix}+\psi_{m3}\begin{bmatrix}\cos 3\theta_e\\ \cos(3\theta_e-3\delta)\\ \cos(3\theta_e-6\delta)\\ \cos(3\theta_e-9\delta)\\ \cos(3\theta_e-12\delta)\end{bmatrix} \quad (1)$$

where ψ_m is the magnetic flux linkage vector, ψ_{m1} and ψ_{m3} represent the amplitudes of the fundamental and third harmonic of the PM flux linkages, θ_e is the rotor electrical position, and δ is the spatial shifting angle between adjacent phases, being $\delta=2\pi/5$.

The fundamental and third harmonic components can be mapped into two orthogonal subspaces, which are decoupled from each other. The fundamental orthogonal subspace is referred as d_1-q_1 and the third harmonic orthogonal subspace is referred as d_3-q_3. The Clarke transformation matrix which transforms the components from the natural coordinate system into the rotating orthogonal coordinate system is shown as follows:

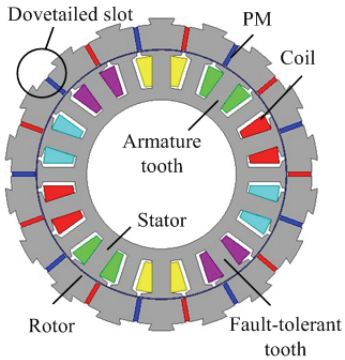

Fig. 1. Cross section of a five-phase PM machine.

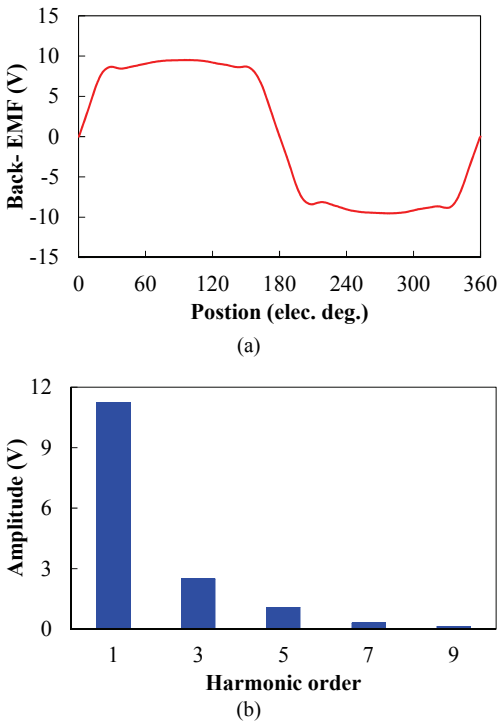

Fig. 2. Measured back-EMF and its THD: (a) Back-EMF, (b) Harmonic order.

TABLE I
Motor Parameters

Symbol	Description	Quantity
ψ_{m1}	Fundamental PM flux linkage	0.0411Wb
ψ_{m3}	3rd harmonic PM flux linkage	0.0033Wb
L_{d1}	Fundamental *d*-axis inductance	0.9323mH
L_{q1}	Fundamental *q*-axis inductance	1.2614mH
P	Pole pairs	9
N_s	Slot number	20

$$T_{Clarke}=\frac{2}{5}\begin{bmatrix}1 & \cos\delta & \cos2\delta & \cos3\delta & \cos4\delta\\ 0 & \sin\delta & \sin2\delta & \sin3\delta & \sin4\delta\\ 1 & \cos3\delta & \cos6\delta & \cos9\delta & \cos12\delta\\ 0 & \sin3\delta & \sin6\delta & \sin9\delta & \sin12\delta\\ \frac{1}{\sqrt{2}} & \frac{1}{\sqrt{2}} & \frac{1}{\sqrt{2}} & \frac{1}{\sqrt{2}} & \frac{1}{\sqrt{2}}\end{bmatrix}. \quad (2)$$

The Park transformation matrix can be presented as follows:

$$T_{Park}=\begin{bmatrix}\cos\theta_e & \sin\theta_e & 0 & 0 & 0\\ -\sin\theta_e & \cos\theta_e & 0 & 0 & 0\\ 0 & 0 & \cos3\theta_e & \sin3\theta_e & 0\\ 0 & 0 & -\sin3\theta_e & \cos3\theta_e & 0\\ 0 & 0 & 0 & 0 & 1\end{bmatrix}. \quad (3)$$

By applying transformation matrices (2) and (3), the *d-q* frame current components of a five-phase PM machine can be presented as:

$$\begin{bmatrix}i_{d1} & i_{q1} & i_{d3} & i_{q3} & i_0\end{bmatrix}=T_{Park}T_{Clarke}I_s \quad (4)$$

where i_{d1}, i_{q1}, i_{d3} and i_{q3} are the current components of the d_1-q_1 axis and the d_3-q_3 axis, and I_s represents the phase current vector.

The stator voltages in the *d-q* frame can be presented as:

$$\begin{bmatrix}u_{d1}\\ u_{q1}\\ u_{d3}\\ u_{q3}\\ u_0\end{bmatrix}=R_s\begin{bmatrix}i_{d1}\\ i_{q1}\\ i_{d3}\\ i_{q3}\\ i_0\end{bmatrix}+\frac{d}{dt}L_{dq}\begin{bmatrix}i_{d1}\\ i_{q1}\\ i_{d3}\\ i_{q3}\\ i_0\end{bmatrix}+p\omega\begin{bmatrix}0\\ \psi_{m1}\\ 0\\ 3\psi_{m3}\\ 0\end{bmatrix} \quad (5)$$

where R_s is the stator resistance, p is the pole pairs, ω is the rotor angular speed, and L_{dq} is the inductance in the *d-q* frame, which can be obtained as follows:

$$L_{dq}=\mathrm{diag}\begin{bmatrix}L_{d1} & L_{q1} & L_{d3} & L_{q3} & L_{ls}\end{bmatrix}=T_{Park}T_{Clarke}L_sT_{Clarke}^{-1}T_{Park}^{-1} \quad (6)$$

where L_{ls} is the leakage inductance, and L_s is the phase inductance matrix.

By taking a derivate of the magnetic co-energy with respect to the rotor mechanical position (θ_m), the torque equation can be obtained as follows:

$$T_e=\frac{\partial W_{co}}{\partial\theta_m}=p\left(\frac{1}{2}I_s^T\frac{\partial L_s}{\partial\theta_e}I_s+I_s^T\frac{\partial\psi_m}{\partial\theta_e}\right) \quad (7)$$

where W_{co} represents the magnetic co-energy.

The electromagnetic torque can be obtained by substituting (1), (4) and (6) into (7):

$$T_e=\frac{5}{2}p\left[\psi_{m1}i_{q1}+3\psi_{m3}i_{q3}+(L_{d1}-L_{q1})i_{d1}i_{q1}+3(L_{d3}-L_{q3})i_{d3}i_{q3}\right]. \quad (8)$$

As expressed in (8), the injection of the third harmonic current improves the output torque.

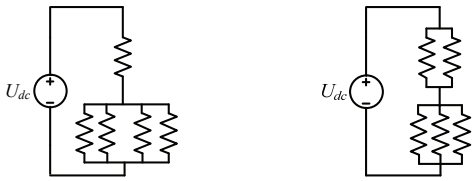

(a) (b)

Fig. 3. Basic equivalent circuit configuration: (a) C14, (b) C23.

III. Proposed Space Vector PWM

A. Switching Vectors in the α-β Frame

The common drive topology of a five-phase PM machine contains a five-phase half-bridge power inverter and a five-phase PM machine. S_A, S_B, S_C, S_D and S_E represent the switching state of phases *A*, *B*, *C*, *D* and *E*, respectively. If the lower switch of phase *x* is ON and the upper switch is OFF, then S_x=0. If the opposite case occurs, then S_x=1.

In a five-phase PWM inverter, there are two different types of basic equivalent circuit configurations, {C14} and {C23}, as shown in Fig. 3. Fig. 3(a) is where one upper switch is ON and four lower switches are OFF or in an opposite manner, like the switching patterns V_{16}(10000) and V_{15}(01111). Fig. 3 (b) is where two upper switches are ON and three lower switches are OFF or in an opposite manner, like the switching patterns V_{24}(11000) and V_7(00111).

By applying a Clarke transformation (2), the DC-link voltage U_{dc} and the switching state of a five-phase inverter, the switching vectors in the α_1-β_1 frame and the α_3-β_3 frame can be obtained as follows:

$$V_{s1}=\frac{2}{5}U_{dc}\left(S_A+\gamma S_B+\gamma^2S_C+\gamma^3S_D+\gamma^4S_E\right) \quad (9)$$

$$V_{s3}=\frac{2}{5}U_{dc}\left(S_A+\gamma S_C+\gamma^2S_E+\gamma^3S_B+\gamma^4S_D\right) \quad (10)$$

where V_{s1} and V_{s3} represent the switching vector in the α_1-β_1 frame and the α_3-β_3 frame, and γ is the rotating factor, being $\gamma=e^{j\delta}$.

There is a total of 2^5=32 switching states in a five-phase inverter. Therefore, there are 32 switching vectors in the α_1-β_1 frame and the α_3-β_3 frame, respectively. According to the magnitudes of the switching vectors, the 32 switching vectors in the α_1-β_1 frame and the α_3-β_3 frame can be classified into large, middle, little and zero switching vectors. The magnitudes of the large, middle and little switching vectors are $0.6472U_{dc}$, $0.4U_{dc}$ and $0.2472U_{dc}$, respectively. There are two zero switching vectors, V_0(00000) and V_{31}(11111). Table II lists the switching vectors in the α_1-β_1 frame and the α_3-β_3 frame. Fig. 4 shows the switching vectors in the α-β frame. As shown in Table II and Fig. 4, the middle vectors in the α_1-β_1 frame and the α_3-β_3 frame belong to C14. The large vectors and little vectors in the α_1-β_1 frame and the α_3-β_3 frame belong to C23. The switching patterns that belong to C23 can

TABLE II
SWITCHING VECTORS GROUPING TABLE

Vectors grouping	Magnitude	α_1-β_1 frame	α_3-β_3 frame
Large vectors	$0.6472U_{dc}$	$V_3,V_6,V_7,V_{12},V_{14},$ $V_{17},V_{19},V_{24},V_{25},V_{28}$	$V_5,V_9,V_{10},V_{11},V_{13},$ $V_{18},V_{20},V_{21},V_{22},V_{26}$
Middle vectors	$0.4U_{dc}$	$V_1,V_2,V_3,V_8,V_{15},$ $V_{16},V_{23},V_{27},V_{29},V_{30}$	$V_1,V_2,V_3,V_8,V_{15},$ $V_{16},V_{23},V_{27},V_{29},V_{30}$
Little vectors	$0.2472U_{dc}$	$V_5,V_9,V_{10},V_{11},V_{13},$ $V_{18},V_{20},V_{21},V_{22},V_{26}$	$V_3,V_6,V_7,V_{12},V_{14},$ $V_{17},V_{19},V_{24},V_{25},V_{28}$
Zero vectors	0	V_0,V_{31}	V_0,V_{31}

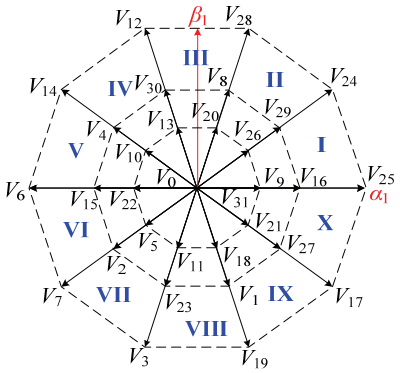

(a)

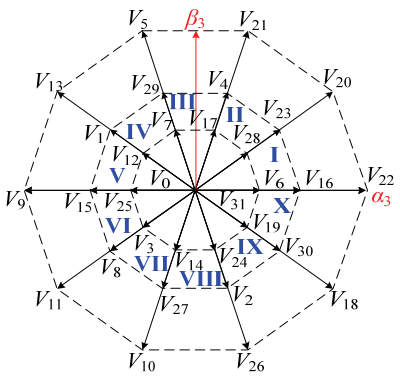

(b)

Fig. 4. Switching vectors in: (a) α_1-β_1 frame, (b) α_3-β_3 frame.

be classified into two categories. The first category is where the three phases with the same switching state are adjacent, which belong to the large vectors in the α_1-β_1 frame and the little vectors in the α_3-β_3 frame. The second category is where the three phases with the same switching state are not adjacent, which belong to the little vectors in the α_1-β_1 frame and the large vectors in the α_3-β_3 frame. In the second category, a phase with the opposite switching state is clamped between three phases with the same switching states. For example, the switching state of phase C is different from the switching states of phases B, D and E in the switching pattern V_{11}(01011). Hence, in the natural coordinate system, the direction of the voltage vector of phase B is opposite the voltage vector composed by phases D and E, which may cause the stator fluxes of the phases to counteract each other. The switching vectors which belong to the little vectors in the α_1-β_1 frame and the large vectors in the α_3-β_3 frame are not recommended.

B. Synthesis of the Reference Vectors

The near four vectors modulation method has been widely used for the control of five-phase PM machines, which can realize a non-sinusoidal phase voltage. This method uses near four vectors to comprise the reference vectors in the α_1-β_1 frame and the α_3-β_3 frame. However, the maximum voltage linear output areas in the α_1-β_1 frame and the α_3-β_3 frame are coupled in this method. When the voltage vector in the α_1-β_1 frame realizes a maximum magnitude of $0.6112U_{dc}$, the maximum magnitude of voltage vector in the α_3-β_3 frame is $0.1453U_{dc}$. When the voltage vector in the α_3-β_3 frame realizes a maximum magnitude of $0.2351U_{dc}$, the maximum magnitude of the voltage vector in the α_1-β_1 frame is $0.3804U_{dc}$.

The novel SVPWM uses the decoupled concept to comprise the reference vectors in the α_1-β_1 frame and the α_3-β_3 frame separately. Then the phase duty cycles corresponding to the reference vectors in the α_1-β_1 frame and the α_3-β_3 frame are calculated. Finally, the calculated phase duty cycles in the α_1-β_1 frame and the α_3-β_3 frame are added to achieve a non-sinusoidal phase voltage.

1) Synthesis of the Reference Vector in the α_1-β_1 Frame

In order to realize the maximum voltage linear output area in the α_1-β_1 frame, ten large vectors and two zero vectors are chosen to comprise the reference voltage in the α_1-β_1 frame. For example, a α_1-β_1 frame reference vector located in sector I, as shown in Fig. 5(a), can be realized by:

$$\begin{cases} |V_{ref1}|\cos\sigma = \dfrac{T_2}{T_S}|V_{25}| + \dfrac{T_1}{T_S}|V_{24}|\cos\dfrac{\pi}{5} \\ |V_{ref1}|\sin\sigma = \dfrac{T_1}{T_S}|V_{24}|\sin\dfrac{\pi}{5} \end{cases} \tag{11}$$

where T_1 and T_2 are the applying times of V_{24} and V_{25}, respectively, and T_s is the sampling time.

T_1, T_2 and the applying time of the zero vectors T_0 can be obtained as follows:

$$\begin{cases} T_1 = \dfrac{|V_{ref1}|\sin\sigma T_S}{|V_{24}|\sin\dfrac{\pi}{5}} \\ T_2 = \dfrac{|V_{ref1}|\sin(\dfrac{\pi}{5}-\sigma)T_S}{|V_{25}|\sin\dfrac{\pi}{5}} \\ T_0 = T_S - T_1 - T_2 \end{cases} \tag{12}$$

Then the duty cycles of phases A, B, C, D and E corresponding to the reference vector in the α_1-β_1 frame can be obtained as follows:

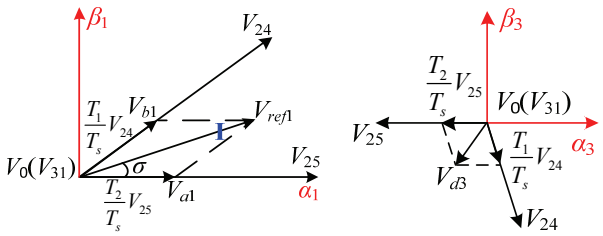

Fig. 5. Realization of a reference voltage vector located in sector I by near two vectors: (a) α_1-β_1 frame, (b) Corresponding vectors in the α_3-β_3 frame.

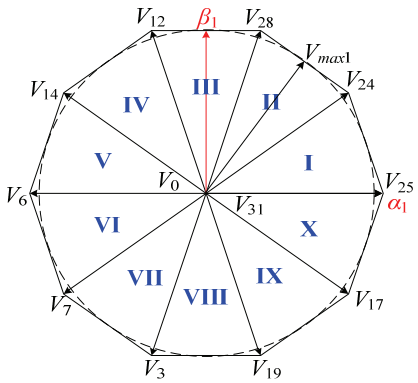

Fig. 6. Trajectory of the voltage vector with the maximum modulation index in the α_1-β_1 frame using the near two vectors method.

$$\begin{cases} duty\_A_1 = 1-\dfrac{T_0}{2T_S}\ ,\ duty\_B_1 = 1-\dfrac{T_0}{2T_S} \\ duty\_C_1 = \dfrac{T_0}{2T_S}\quad ,\ duty\_D_1 = \dfrac{T_0}{2T_S}\quad . \\ duty\_E_1 = \dfrac{T_0}{2T_S}+\dfrac{T_2}{T_S} \end{cases} \tag{13}$$

The trajectory of the voltage vector in the α_1-β_1 frame with the maximum magnitude in the linear modulation region can be drawn as the inscribed circle of the decagon consisting of ten large vectors, as shown in Fig. 6. Then the maximum modulation index of this method can be calculated as:

$$m_{\max 1} = \frac{V_{Large}}{U_{dc}}\cos\frac{\pi}{10} = 0.6155. \tag{14}$$

The near two vectors method can realize the maximum magnitude of a voltage vector in the linear modulation region. In the α_3-β_3 frame, the V_{d3} shown in Fig. 5(b) is comprised by V_{24} and V_{25}. In the traditional near two vectors method, due to the vector in the α_3-β_3 frame without control, V_{d3} produces an uncontrolled third harmonic component. In the proposed SVPWM, V_{d3} is considered as a disturbance in the α_3-β_3 frame. Since the vector in the α_3-β_3 frame is close-loop controlled, the disturbance V_{d3} can be restrained.

2) Synthesis of the Reference Vector in the α_3-β_3 Frame

The ten large vectors in the α_3-β_3 frame will cause the stator

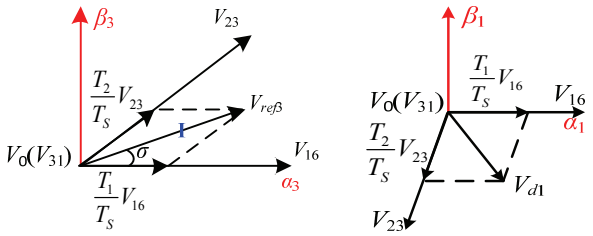

Fig. 7. Realization of a reference voltage vector located in sector I by near two middle vectors: (a) In the α_3-β_3 frame, (b) The corresponding vector in the α_1-β_1 frame.

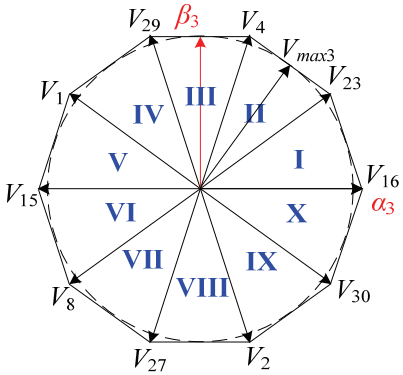

Fig. 8. Trajectory of the voltage with the maximum modulation index in the α_3-β_3 frame using the near two vectors method.

fluxes of the phases to counteract each other, which has been explained in Section III part A. Hence, the ten large vectors in the α_3-β_3 frame are not recommended for use. The ten middle vectors, ten little vectors and two zero vectors can be used to comprise the reference vector in the α_3-β_3 frame.

a) Near Two Vectors Method in the α_3-β_3 Frame

To realize the maximum voltage linear output area in the α_3-β_3 frame, the ten middle vectors and two zero vectors are chosen to comprise the reference voltage in α_3-β_3 frame. The calculation method of applying time of near two middle vectors in the α_3-β_3 frame is similar to the method in the α_1-β_1 frame. For example, the reference vector located in sector I is comprised by V_{16} and V_{23} in the α_3-β_3 frame, as shown in Fig. 7.

The duty cycles of phases A, B, C, D and E corresponding to the reference vector located in sector I under the α_3-β_3 frame can be obtained as follows:

$$\begin{cases} duty\_A_3 = 1-\dfrac{T_0}{2T_S}\quad ,\ duty\_B_3 = \dfrac{T_0}{2T_S} \\ duty\_C_3 = \dfrac{T_0}{2T_S}+\dfrac{T_2}{T_S}\ ,\ duty\_D_3 = \dfrac{T_0}{2T_S}+\dfrac{T_2}{T_S} \\ duty\_E_3 = \dfrac{T_0}{2T_S}+\dfrac{T_2}{T_S} \end{cases} \tag{15}$$

where T_0, T_1 and T_2 are the applying times of the zero vectors, V_{16} and V_{23}, respectively.

The trajectory of the voltage vector in the α_3-β_3 frame with

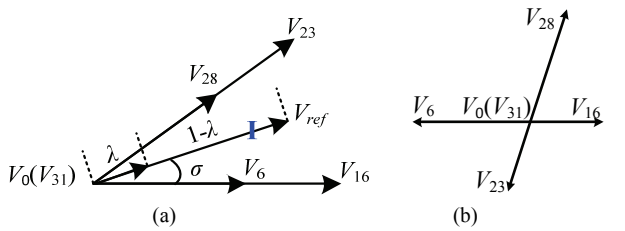

Fig. 9. Realization of a reference voltage vector located in sector I by near four vectors: (a) In the α_3-β_3 frame, (b) The corresponding vector in the α_1-β_1 frame.

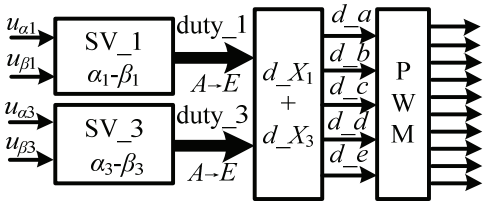

Fig. 10. Diagram of the proposed SVPWM.

the maximum magnitude in the linear modulation region can be drawn as the inscribed circle of the decagon consisting of ten middle vectors shown in Fig. 8. The maximum modulation index of this method can be calculated as:

$$m_{\max 3} = \frac{V_{Middle}}{U_{dc}} \cos\frac{\pi}{10} = 0.3804. \tag{16}$$

In the α_1-β_1 frame, the V_{d1} shown in Fig. 7(b) is comprised by V_{16} and V_{23}. In the proposed SVPWM, V_{d1} is also considered as a disturbance in the α_1-β_1 frame. The disturbance V_{d1} can be restrained, due to the closed-loop control of the vector in the α_1-β_1 frame.

b) Near Four Vectors Method in the α_3-β_3 Frame

The near two vectors method mentioned above can realize the maximum magnitude of a voltage vector in the linear modulation region in the α_3-β_3 frame. However, it produces a disturbance vector in the α_1-β_1 frame. In order to improve the robustness of the system, the near four vectors method can be adopted.

This method chooses the near four vectors (two middle and two little vectors) to comprise the reference vector in the α_3-β_3 frame. For example, the reference vector located in sector I is comprised by V_6, V_{16}, V_{23} and V_{28} in the α_3-β_3 frame, as shown in Fig. 9. In addition, T_1, T_2, T_3 and T_4 are applying times of V_6, V_{16}, V_{23} and V_{28}, respectively. In order for the value of the vector comprised in the α_1-β_1 frame to be zero, the applying time of the middle vectors and little vectors should satisfy the following equation:

$$\frac{T_{Middle}}{T_{Little}} = \frac{T_2}{T_1} = \frac{T_3}{T_4} = 1.618. \tag{17}$$

In the α_3-β_3 frame, V_6 and V_{28} are used to comprise λV_{ref3}, and V_{16} and V_{23} are used to comprise $(1\text{-}\lambda)V_{ref3}$. In addition, λ can be calculated by the following equation:

$$\frac{(1-\lambda)\left|V_{ref3}\right|/0.4U_{dc}}{\lambda\left|V_{ref3}\right|/0.2472U_{dc}} = \frac{T_2}{T_1} = 1.618 \tag{18}$$

where λ=0.2764.

T_1, T_2, T_3, T_4 and the applying time of the zero vectors T_0 can be obtained as follows:

$$\begin{cases} T_1 = \dfrac{0.2764\left|V_{ref3}\right|\sin(\frac{\pi}{5}-\sigma)T_S}{\left|V_6\right|\sin\frac{\pi}{5}}, T_3 = \dfrac{0.7236\left|V_{ref3}\right|\sin\sigma T_S}{\left|V_{23}\right|\sin\frac{\pi}{5}} \\ T_2 = \dfrac{0.7236\left|V_{ref3}\right|\sin(\frac{\pi}{5}-\sigma)T_S}{\left|V_{16}\right|\sin\frac{\pi}{5}}, T_4 = \dfrac{0.2764\left|V_{ref3}\right|\sin\sigma T_S}{\left|V_{28}\right|\sin\frac{\pi}{5}} \\ T_0 = T_S - T_1 - T_2 - T_3 - T_4 \end{cases} \tag{19}$$

The duty cycles of phases A, B, C, D and E corresponding to the reference vector in the α_3-β_3 frame in this method can be obtained as follows:

$$\begin{cases} duty\_A_3 = 1 - \dfrac{T_0}{2T_S} - \dfrac{T_1}{T_S}, \; duty\_B_3 = \dfrac{T_0}{2T_S} + \dfrac{T_4}{T_S} \\ duty\_C_3 = 1 - \dfrac{T_0}{2T_S} - \dfrac{T_2}{T_S}, \; duty\_D_3 = \dfrac{T_0}{2T_S} + \dfrac{T_1}{T_S} + \dfrac{T_3}{T_S}. \\ duty\_E_3 = \dfrac{T_0}{2T_S} + \dfrac{T_3}{T_S} \end{cases} \tag{20}$$

The maximum voltage vector of this method which uses the near four vectors to comprise the vector in the α_3-β_3 frame can be obtained as follows:

$$V_{\max 3} = \left(\frac{1}{1+1.618}\times 0.2472U_{dc} + \frac{1.618}{1+1.618}\times 0.4U_{dc}\right)\cos\frac{\pi}{10} = 0.3249U_{dc}. \tag{21}$$

The maximum modulation index in the α_3-β_3 frame of this method is presented as follows:

$$m_{\max 3} = \frac{V_{\max 3}}{U_{dc}} = 0.3249. \tag{22}$$

3) Generation of the Switching Signals

The total duty cycles of the phases can be obtained as follows:

$$duty\_X = duty\_X_1 + duty\_X_3 - 0.5 \tag{23}$$

where X is A, B, C, D and E.

Then the switching signal of every phase can be modulated by the corresponding duty cycle and triangular carrier. The maximum value of the triangle carrier is 1, and the minimum value is 0. The frequency of the triangle carrier can be selected according to the maximum frequency of the inverter.

In the methods mentioned above (section III part B (1) and (2)), the switching vectors used to comprise the reference vectors in the α_1-β_1 frame and the α_3-β_3 frame are decoupled. The method using the near two vectors in the α_1-β_1 frame and the α_3-β_3 frame is denoted as Method I, the method using the near two vectors in the α_1-β_1 frame and the near four vectors in the α_3-β_3 frame is denoted as Method II. Method I can realize the maximum magnitude of the voltage vector in the linear modulation region under the α_1-β_1 frame and the α_3-β_3

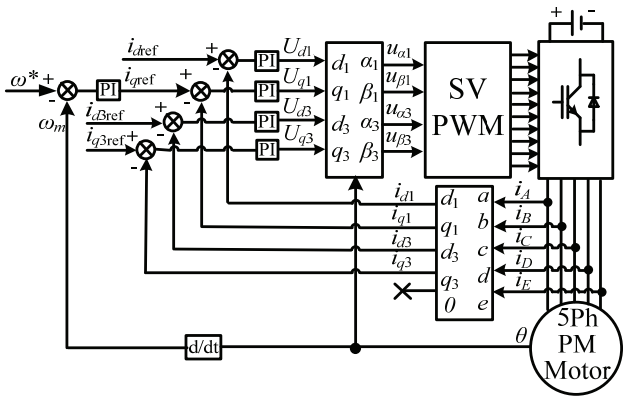

Fig. 11. Control scheme with the proposed SVPWM method.

frame, respectively. Method II can improve the robustness of the system on the basis of ensuring the maximum modulation index in the α_1-β_1 frame. A diagram of the proposed SVPWM is shown in Fig. 10.

IV. Verification

A. Simulated Results

To evaluate the performance of the proposed SVPWM strategy, a simulation model of a five-phase PM machine drive is developed. Fig. 11 shows a schematic of the five-phase PM machine drive control system including the proposed SVPWM method, which can realize the control of the objective in the α_3-β_3 frame. The SVPWM block in Fig. 11 is detailed in Fig. 10. Fig. 12 shows the reference current and sampled current of phase A using Method I and Method II under same operation condition. The simulated results show that the two proposed SVPWM methods can regulate non-sinusoidal phase currents including the third harmonic component without steady-state error.

B. Experimental Results

In order to verify the suitability of the proposed SVPWM, a test platform has been set up as shown in Fig. 13. The experimental set is composed of a five-phase PM machine, a five-phase half-bridge inverter, and a DC generator as the load. A dSPACE1005 controller is utilized for the implementation of the overall control algorithm. The machine torque is measured by a high precision torque transducer (HBM T20WN/20NM). The frequency of the IGBTs is fixed at 10 kHz, and the DC-link voltage is 60 V.

Fig. 14 shows the torque and phase current waveforms using Method I. The load torque is 6.2 Nm. Fig. 15 shows the sampled and reference current components in the d_1-q_1 axis and the d_3-q_3 axis. In addition, i_{d1}, i_{q1}, i_{d3} and i_{q3} represent the sampled current components of the d_1-q_1 axis and the d_3-q_3 axis, respectively. Meanwhile, i_{q1r} and i_{q3r} are the reference currents of the q_1-axis and the q_3-axis, respectively. In this experiment, the reference currents of the d_1-axis and the

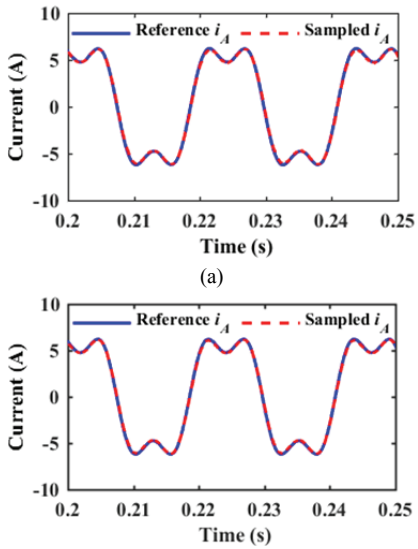

Fig. 12. The waveforms of the phase A reference current and sampled current using: (a) Method I, (b) Method II.

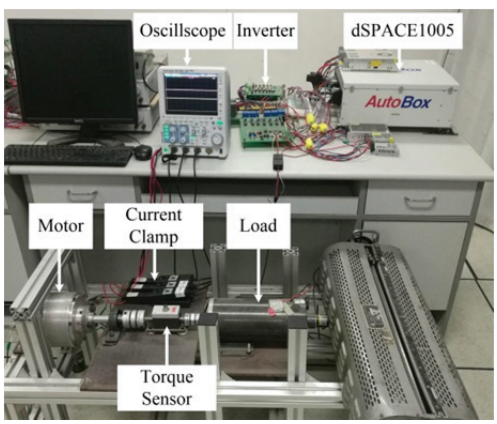

Fig. 13. Experimental test platform.

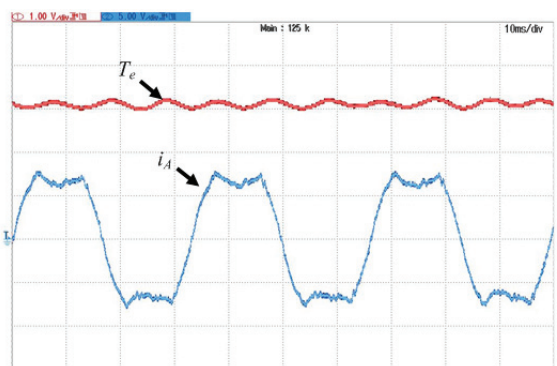

Fig. 14. Torque and phase current waveforms using Method I; T_e is scaled to 2 Nm/div, the phase current is scaled to 5A/div.

d_3-axis are 0 and the reference current in the q_3-axis is 2 A. In this experiment, the q_1-axis current i_{q1} is 8.7 A. The q_3-axis reference current can be calculated by multiplying i_{q1} by the ratio of the third harmonic 22.2% [10]. The result is about

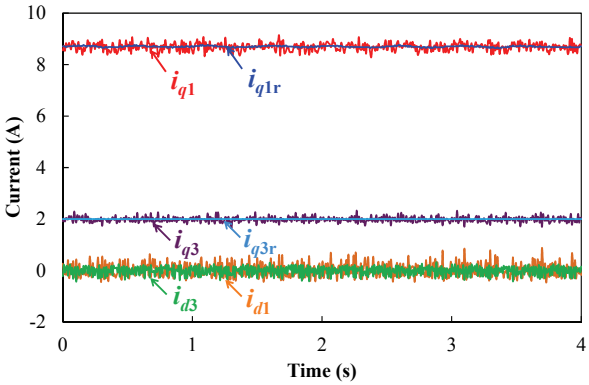

Fig. 15. Sampled and reference current components in the d_1-q_1 axis and the d_3-q_3 axis using Method I.

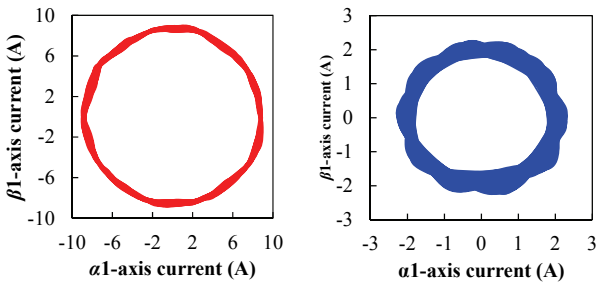

Fig. 16. Trajectories of the sampled current vectors using Method I in the: (a) α_1-β_1 axis, (b) α_3-β_3 axis.

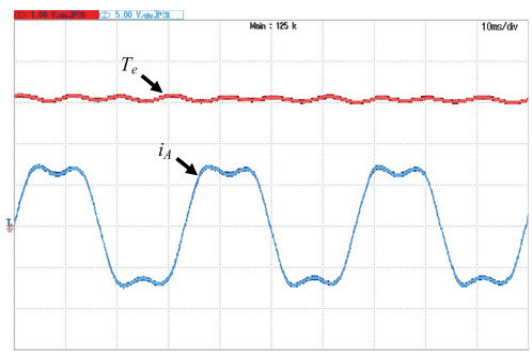

Fig. 17. Torque and phase current waveforms using Method II; T_e is scaled to 2 Nm/div, the phase current is scaled to 5A/div.

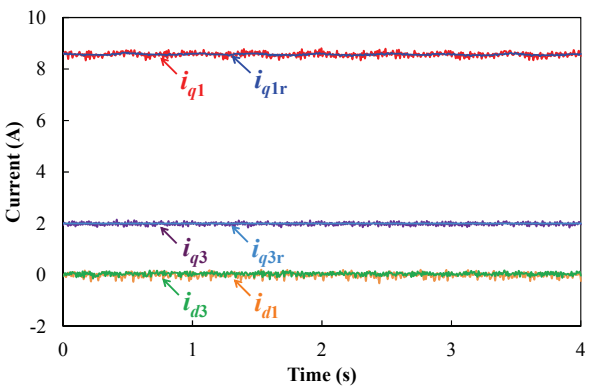

Fig. 18. Sampled and reference current components of the d_1-q_1 axis and the d_3-q_3 axis using Method II.

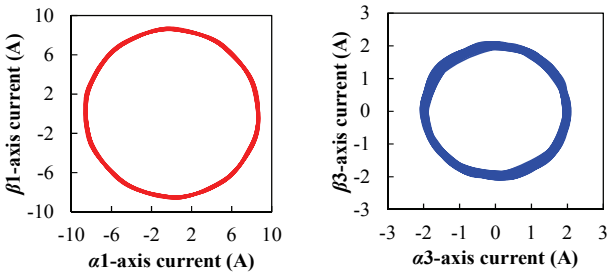

Fig. 19. Trajectories of the sampled current vectors using Method II in the: (a) α_1-β_1 axis, (b) α_3-β_3 axis.

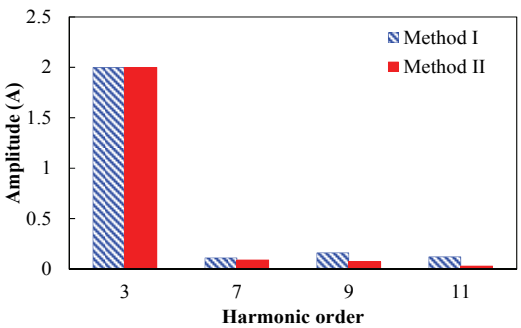

Fig. 20. Amplitude of the harmonic currents.

equal to 2 A. The reference current of the q_3-axis is set as 2 A, which can improve the output torque and is also convenient for checking the value of the feedback current i_{q3}. As shown in Fig. 15, the sampled currents can track the reference currents accurately in the d_1-q_1 axis and the d_3-q_3 axis. Fig. 16 shows trajectories of the sampled current vectors in the α_1-β_1 axis and α_3-β_3 axis. The experimental results (Figs. 14-16) reveal that non-sinusoidal phase currents, including the third harmonic component, can be regulated without steady-state error by employing Method I.

Fig. 17 exhibits torque and phase current waveforms using Method II. Fig. 18 shows the sampled and reference current components of the d_1-q_1 axis and the d_3-q_3 axis. The reference current components of the d_1-axis and the d_3-axis are 0, and the reference current of the q_3-axis is 2 A. As shown in Fig. 18, the sampled current can track the reference currents accurately in the d_1-q_1 axis and the d_3-q_3 axis. Fig. 19 shows the trajectories of the sampled current vectors in the α_1-β_1 axis and the α_3-β_3 axis. Experimental results (Figs. 17-19) show that Method II can realize control of the third harmonic current without steady-state error.

Comparing the experimental results of Fig. 15 and Fig. 18, the current ripples of Method II are less than those of Method I in the d_1-q_1 axis and the d_3-q_3 axis. Fig. 20 shows fast Fourier transformation results of the phase current using Method I and Method II. The fundamental currents of Method I and Method II are 8.7 A and 8.5 A, respectively. The third harmonic currents of both methods are 2 A, which are equal to the reference values. As shown in Fig. 20, the amplitudes of the seventh, ninth and eleventh harmonic

currents in Method II are less than those in Method I. By comparing experimental results of Method I and Method II, it can be condluded that the experimental effectiveness of Method II is better than that of Method I. This conclusion is consistent with the theoretical analysis mentioned above (Section III part B (3)).

V. CONCLUSIONS

In this paper, a novel decoupled SVPWM has been proposed to realize a non-sinusoidal phase voltage. In the α_1-β_1 frame, the reference vector has been comprised by near two large vectors to guarantee the maximum voltage linear output area. The corresponding vector comprised by two vectors in the α_3-β_3 frame has been considered as a disturbance, which has been restrained by close-loop control. In the α_3-β_3 frame, there are two methods of comprising the reference vector. For Method I, near two middle vectors have been used to maintain the maximum voltage linear output area in the α_3-β_3 frame. For Method II, near four vectors (two middle and two little vectors) have been adopted to improve the robustness of the system on the basis of ensuring the maximum modulation index in the α_1-β_1 frame. In the proposed method, the switching vectors used to comprise the reference vectors in the α_1-β_1 frame and the α_3-β_3 frame are decoupled, which can guarantee the maximum modulation index in the α_1-β_1 frame. The proposed SVPWM has been experimentally verified. Both of these results demonstrate that the proposed SVPWM can regulate non-sinusoidal phase current including the third harmonic component without steady-state error.

REFERENCES

[1] G. J. Li, B. Ren, and Z. Q. Zhu, "Design guidelines for fractional slot multi-phase modular permanent magnet machines," *IET Electr. Power Appl.*, Vol. 11, No. 6, pp. 1023-1031, Jul. 2017.

[2] X. Deng, B. Mecrow, H. Wu, and R. Martin, "Design and development of low torque ripple variable-speed drive system with six-phase switched reluctance motors," *IEEE Trans. Energy Conv.*, Vol. 33, No. 1, pp. 420-429, Mar. 2018.

[3] S. S. R. Bonthu, S. Choi, and J. Baek, "Design optimization with multi-physics analysis on external rotor permanent magnet assisted synchronous reluctance motors," *IEEE Trans. Energy Conv.*, Vol. 33, No. 1, pp. 290-298, Mar. 2018.

[4] A. S. Abdel-Khalik, S. Ahmed and A. M. Massoud, "Dynamic modeling of a five-phase induction machine with a combined star/pentagon stator winding connection," *IEEE Trans. Energy Conv.*, Vol. 31, No. 4, pp. 1645-1656, Dec. 2016.

[5] F. Scuiller, H. Zahr, and E. Semail, "Maximum reachable torque, power and speed for five-phase SPM machine with low armature reaction," *IEEE Trans. Energy Conv.*, Vol. 31, No. 3, pp. 959-969, Sep. 2016.

[6] K. Wang, Z. Y. Gu, Z. Q. Zhu, and Z. Z. Wu, "Optimum injected harmonics into magnet shape in multiphase surface-mounted PM machine for maximum output torque," *IEEE Trans. Ind. Electron.*, Vol. 64, No. 6, pp. 4434-4443, Jun. 2017.

[7] K. Wang, Z. Q. Zhu, and G. Ombach, "Torque improvement of five-phase surface-mounted permanent magnet machine using third-order harmonic," *IEEE Trans. Energy Conv.*, Vol. 29, No. 3, pp. 735-747, Sep. 2014.

[8] F. Scuiller, "Magnet shape optimization to reduce pulsating torque for a five-phase permanent-magnet low-speed machine," *IEEE Trans. Magn.*, Vol. 50, No. 4, pp. 1-9, Apr. 2014.

[9] L. Parsa and H. A. Toliyat, "Five-phase permanent-magnet motor drives," *IEEE Trans. Ind. Appl.*, Vol. 41, No. 1, pp. 30-37, Jan./Feb. 2005.

[10] Z. Y. Gu, K. Wang, Z. Q. Zhu, Z. Z. Wu, C. Liu, and R. W. Cao, "Torque improvement in five-phase unequal tooth SPM machine by injecting third harmonic current," *IEEE Trans. Veh. Technol.*, Vol. 67, No. 1, pp. 206-215, Jan. 2018.

[11] M. J. Duran, F. Salas, and M. R. Arahal, "Bifurcation analysis of five-phase induction motor drives with third harmonic injection," *IEEE Trans. Ind. Electron.*, Vol. 55, No. 5, pp. 2006-2014, May 2008.

[12] H. Xu, H. A. Toliyat, and L. J. Petersen, "Five-phase induction motor drives with DSP-based control system," *IEEE Trans. Power Electron.*, Vol. 17, No. 4, pp. 524-533, Jul. 2002.

[13] H. A. Toliyat, T. A. Lipo, and J. C. White, "Analysis of a concentrated winding induction machine for adjustable speed drive applications part 2 (motor design and performance)," *IEEE Trans. Energy Conv.*, Vol. 6, No. 4, pp. 684-692, Dec. 1991.

[14] H. A. Toliyat, T. A. Lipo, and J. C. White, "Analysis of a concentrated winding induction machine for adjustable speed drive applications-experimental results," *IEEE Trans. Energy Conv.*, Vol. 9, No. 4, pp.695-700, Dec. 1994.

[15] R. Shi and H. A. Toliyat, "Vector control of five-phase synchronous reluctance motor with space vector pulse width modulation (SVPWM) for minimum switching losses," *in Proc. IEEE Appl. Power Electron. Conf. (APEC).*, pp. 57-63, 2002.

[16] J. Prieto, M. Jones, F. Barrero, E. Levi, and S. Toral, "Comparative analysis of discontinuous and continuous PWM techniques in VSI-fed five-phase induction motor," *IEEE Trans. Ind. Electron.*, Vol. 58, No. 12, pp. 5324-5335, Dec. 2011.

[17] P. S. N. de Silva, J. E. Fletcher and B. W. Williams, "Development of space vector modulation strategies for five phase voltage source inverters," in *Proc. Inst. Electr. Eng. Power electr. Drives Conf. (PEMD).*, pp. 650-655, 2004.

[18] M. J. Duran, J. Prieto, F. Barrero, J. A. Riveros, and H. Guzman, "Space-vector PWM with reduced common-mode voltage for five-phase induction motor drives," *IEEE Trans. Ind. Electron.*, Vol. 60, No. 10, pp. 4159-4168, Oct. 2013.

[19] M. J. Duran, J. Prieto, and F. Barrero, "Space vector PWM with reduced common-mode voltage for five-phase induction motor drives operating in overmodulation zone," *IEEE Trans. Power Electron.*, Vol. 28, No. 8, pp. 4030-4040, Aug. 2013.

[20] M. Jones, E. Levi, D. Dujic, J. Prieto, and F. Barrero, "Current ripple in inverter-fed five-phase drives with space-vector PWM," *IEEE Inter. Symp. Ind. Electron. (ISIE).*, pp. 2153-2159, 2010.

[21] H. M. Ryu, J. H. Kim, and S. K. Sul, "Analysis of multiphase space vector pulse-width modulation based on multiple *d-q* spaces concept," *IEEE Trans. Power Electron.*,

Vol. 20, No. 6, pp. 1364-1371, Nov. 2005.
[22] Q. Chen, G. Liu, W. Zhao, L. Sun, M. Shao, and Z. Liu, "Design and comparison of two fault-tolerant interior-permanent-magnet motors," *IEEE Trans. Ind. Electron.*, Vol. 61, No. 12, pp. 6615-6623, Dec. 2014.

Zhipeng Lin received his B.S. degree in Control Engineering from Jiangsu University, Zhenjiang, China, in 2016, where, he is presently working towards his M.S. degree in Control Science and Engineering. His current research interests include the power-electric control of electric machines and fault tolerant control.

Guohai Liu received his B.S. degree in Electrical Engineering from Jiangsu University, Zhenjiang, China, in 1985; and his M.S. and Ph.D. degrees in Control Engineering from Southeast University, Nanjing, China, in 1988 and 2002, respectively. Since 1988, he has been with Jiangsu University, where he is presently working as a Professor and as the Dean of the School of Electrical Information Engineering. From 2003 to 2004, he was a Visiting Professor in the Department of Electronic and Electrical Engineering, University of Sheffield, Sheffield, ENG, UK. His current teaching and research interests include electrical machines, motor drives for electric vehicles and intelligent control. He has authored or coauthored over 200 technical papers and 4 textbooks in these areas. He also holds 30 chinese patents. Dr. Liu is a Fellow of the IET.

Wenxiang Zhao received his B.S. and M.S. degrees in Electrical Engineering from Jiangsu University, Zhenjiang, China, in 1999 and 2003, respectively; and his Ph.D. degree in Electrical Engineering from Southeast University, Nanjing, China, in 2010. Since 2003, he has been with Jiangsu University, where he is presently working as a Professor in the School of Electrical Information Engineering. From 2008 to 2009, he was a Research Assistant in the Department of Electrical and Electronic Engineering, University of Hong Kong, Hong Kong, China. From 2013 to 2014, he was a Visiting Professor in the Department of Electronic and Electrical Engineering, University of Sheffield, Sheffield, ENG, UK. His current research interests include electric machine design, modeling, fault analysis, and intelligent control. He has authored and co-authored over 130 technical papers in these areas.

Qian Chen received his B.S. degree in Electrical Engineering and his Ph.D. degree in Control Engineering from Jiangsu University, Zhenjiang, China, in 2009 and 2015, respectively. Since 2015, he has been with Jiangsu University, where he is presently working as an Associate Professor in the School of Electrical Information Engineering. His current research interests include electric machine design, modeling, fault analysis, and intelligent control.